Atmos. Chem. Phys. Discuss., 14, 3169–3191, 2014
www.atmos-chem-phys-discuss.net/14/3169/2014/
doi:10.5194/acpd-14-3169-2014

Atmospheric Chemistry and Physics Discussions

Enhancement of aerosols in UTLS over the Tibetan Plateau induced by deep convection during the Asian summer monsoon

Q. S. He[1], C. C. Li[2], J. Z. Ma[3], H. Q. Wang[4], X. L. Yan[3], Z. R. Liang[1], and G. M. Qi[5]

[1]Shanghai Meteorological Service, Shanghai, China
[2]Department of Atmospheric and Oceanic Sciences, School of Physics, Peking University, Beijing, China
[3]Chinese Academy of Meteorological Sciences, Beijing, China
[4]College of Environmental Science and Engineering, Donghua University, Shanghai, China
[5]Germu Meteorological Bureau, Qinghai, China

Received: 6 November 2013 – Accepted: 6 January 2014 – Published: 31 January 2014

Correspondence to: C. C. Li (ccli@pku.edu.cn)

Published by Copernicus Publications on behalf of the European Geosciences Union.

Abstract

Vertical profiles of aerosol extinction coefficients were measured by an Micro Pulse Lidar at Naqu (31.5° N, 92.1° E, 4508 m a.m.s.l.), a meteorological station located on the central part of the Tibetan Plateau during summer 2011. Observations show a persistent maximum in aerosol extinction coefficients in the upper troposphere–lower stratosphere (UTLS) within an anticyclone during the Asian summer monsoon. These aerosol layers were generally located at an altitude of 18–19 km m.s.l., 1–2 km higher than the tropopause, with broad layer depth ranging approximately 3–4 km. Variations in these aerosols are found to be closely related to the intensity of underlying deep convection. Efficient vertical transport resulting from the most intensive convection is considered to be most important for the enhancement of aerosols observed near the tropopause. Temporal variations in aerosol layer in UTLS over the Plateau show a significant peak at midnight. This further indicates that deep convection plays an important role in the accumulation of aerosols in UTLS over the Tibetan Plateau.

1 Introduction

Aerosols in the upper troposphere–lower stratosphere (UTLS) play an important role in the global/regional climate system and the geochemical cycle (Hanson et al., 1994; Borrmann et al., 1997; Solomon et al., 1997). They also influence atmospheric ozone budgets through providing surface areas for efficient heterogeneous reactions (Keim et al., 1996; Solomon, 1999). Using the Stratospheric Aerosol and Gas Experiment II (SAGE II) data, Li et al. (2001) found that aerosol concentrations near 100 hPa are higher over the Tibetan Plateau than over China's central and northern regions in summer. Recent observations by balloon-borne optical particle counter (Tobo et al., 2007) and aircraft-borne measurements (Keim et al., 1996; Solomon, 1997) showed that soot-containing liquid aerosols with the major components of fine particles may also affect the aerosol layer near the tropopause. Appearance of cold tropopause in

ACPD
14, 3169–3191, 2014

the upper troposphere (possibly in the lower stratosphere also) has been considered as an important factor to explain the enhancement of tropopause aerosols observed in summer over the Plateau (Kim et al., 2003). This observational fact is important from the point view of heterogeneous reactions on aerosol surfaces since gas-to-particle conversion processes are generally more active in low temperature. During summer, the elevated surface heating and rising air associated with persistent deep convection over the Tibetan Plateau leads to anticyclonic circulation and divergence in the UTLS (Yanai et al., 1992; Hoskins and Rodwell, 1995; Highwood and Hoskins, 1998), where persistently enhanced pollutants such as aerosols, CO, methane and nitrogen oxides, as well as water vapor, can be linked to the rapid vertical transport of surface air from Asia, India and Indonesia in deep convection and confinement by strong anticyclonic circulation (Rosenlof et al., 1997; Jackson et al., 1998; Dethof et al., 1999; Park et al., 2004; Filipiak et al., 2005; Li et al., 2005a; Fu et al., 2006). Because the main outflow of deep convection occurs near 12 km a.m.s.l. altitude, well below the tropopause level (16 km a.m.s.l.), how aerosols with an origin from the lower troposphere attain altitudes as high as 16 km is still not well understood. A clarification of the mechanisms of aerosol transport into the UTLS over this region is an important step toward understanding tropospheric influences on hydration and chemical composition in the global stratosphere. Knowing the height dependence of the aerosol changes is important for understanding the mechanisms responsible for the transport of aerosols from the troposphere to the stratosphere over the Tibetan Plateau; however, a variety of aerosol vertical distributions and optical properties over the Tibetan Plateau has not been assessed in a satisfactory manner due to lack of continuous direct observations.

The vertical distributions of aerosol extinction coefficients were measured over the Tibetan Plateau in the summer of 2011, as part of the project "Tibetan Ozone, Aerosol and Radiation" (TOAR). In this study, the lidar and radiosonde measurement results are presented and compared with satellite data. We find a persistent maximum in aerosol extinction coefficients in the UTLS within the anticyclone, and show that such aerosol accumulation can be linked to the development of the Tibetan deep convective sys-

ACPD
14, 3169–3191, 2014

tems. These results indicate that deep convection could primarily affect aerosol and hence radiation properties near the tropopause over the Tibetan Plateau.

2 Measurements and data

2.1 Micro Pulse Lidar

An Micro Pulse Lidar (MPL-4B, Sigma Space Corp., USA) was operated at the Naqu Meteorological Bureau (31.5° N, 92.1° E, 4508 m m.s.l.) on the central part of the Tibetan Plateau. The MPL is a backscatter lidar which uses an Nd:YLF laser with an output power of 12 µJ at 532 nm and 2500 Hz repetition rate. The diameter of the receiving telescope is 20 cm, and the field of view is 0.1 mrad. The vertical resolution of the lidar observation is 30 m, and the integration time is 30 s. Data obtained on the cloud-free days during nighttime were selected in order to avoid the disturbance of cloud and/or rain to column-averaged lidar ratio and solar noise.

In general, the inversion of the LIDAR profile is based on the solution of the single scattering LIDAR equation:

$$P(r) = O_c(r) C E \frac{\beta(r)}{r^2} \exp\left[-2\int_0^r \sigma(z)\mathrm{d}z\right] \quad (1)$$

where r is the range, $\beta(r)$ represents the total backscattering coefficient $\beta(r) = \beta_m(r) + \beta_a(r)$, $\sigma(r)$ is the total extinction coefficient $\sigma(r) = \sigma_m(r) + \sigma_a(r)$, C is the LIDAR constant, which incorporates the transmission and the detection efficiency, and E is the laser pulse energy. $\beta_a(r)$ and $\sigma_a(r)$ are aerosol backscattering and extinction coefficients, respectively. $\beta_m(r)$ and $\sigma_m(r)$ are molecular contributions to the backscattering and the extinction coefficients, respectively. They can be evaluated by the Rayleigh-scattering theory from the Standard Atmosphere 1976 (NASA, 1976). But here the molecular extinction coefficients are evaluated using temperature and pressure from

ACPD
14, 3169–3191, 2014

the radiosondes that released at the lidar field site twice a day. $O_c(r)$ is the overlap correction as a function of the range caused by field-of-view conflicts in the transceiver system. Systematic errors of $P(r)$ were mainly observed in the lowest altitudes where an incomplete overlap between the emitted laser beam and the telescope field-of-view can led to an underestimation of aerosol backscatter and extinction coefficients. Since the majority of aerosols are contained in the first several kilometers of the atmosphere, the overlap problem must be solved. Overlap is typically solved experimentally, using techniques outlined by Campbell et al. (2002). The starting point is an averaged data sample where the system is pointed horizontally with no obscuration. By choosing a time when the atmosphere is well mixed, such as late afternoon, or, even better, when the aerosol loading is low, backscattering through the layer is roughly assumed to be constant with range (i.e., the target layer is assumed to be homogeneous). The similar overlap calibration was carried out at the beginning of this field experiment.

The vertical profile of aerosol extinction coefficient σ_a is determined by a near end approach in solving the lidar equation as proposed by Fernald (1984). The column averaged lidar ratios are estimated by constraining the vertical integral of lidar-derived aerosol extinction coefficients with independent aerosol optical depth measurements by the collocated sunphotometer (Welton et al., 2000; Chazette, 2003). The averaged column averaged lidar ratios are approximately 30 sr from all measurement examples. We identify the boundaries of aerosol layer in the UTLS from the lidar extinction coefficient profiles. The lowest bin with $\sigma_a = 0.001\ \mathrm{km}^{-1}$ above 18 km is identified as the top of aerosol layer H_t and the bin with minimum value of σ_s between 10 km and 16 km as the layer base H_b. The visible optical depth of the aerosol layer is derived by integrating the values of σ_a between H_b and H_t.

2.2 Radiosonde observations

During the field campaigns, 76 L-band (GTS1) electronic radiosondes (Nanjing Bridge Machinery Co., Ltd., China) were launched to provide vertical profiles of pressure, tem-

ACPD
14, 3169–3191, 2014

perature, and humidity up to 25 km to 30 km high. The radiosondes were released at the lidar field site in Naqu twice a day at 00:00 and 12:00 UTC.

11 weather balloons with Vaisala RS92 radiosondes (Vömel et al., 2007) have been launched to provide profiles of air temperature, relative humidity RH, wind speed and wind direction usually up to the mid stratosphere. The RH can be measured between 0 and 100 % with a resolution of 1 % and an accuracy of 5 % at −50 °C (Miloshevich et al., 2006; Währn et al., 2004).

2.3 Satellite observations

National Oceanic and Atmospheric Administration (NOAA) satellites provide an outgoing longwave radiation (OLR) product for the top of the atmosphere. OLR data are calculated on a daily basis by the Climate Diagnostic Center (CDC), a division of NOAA (Liebmann and Smith, 1996). The horizontal resolution is 2.5° by 2.5°. Missing values are computed by applying spatial and temporal interpolations. The OLR in this data set is calculated by converting 10 µm to 12 µm channel radiances measured by the Advanced High Resolution Radiometer aboard the NOAA operational polar orbiting satellites. The daily mean is the average of one daytime and one nighttime measurement. The OLR emitted by high, cold, deep convective clouds is much lower than that by warm low clouds or by the Earth's surface. Usually, values of less than 200 $W m^{-2}$ indicate deep convection (Fujiwara et al., 2009). Deep convection, in turn, indicates the regions with extensive lifting of air that may act as source regions for aerosol layer.

We used the water vapor profiles observations (version 3.3) from the Microwave Limb Sounder (MLS) on the NASA Aura satellite (Waters et al., 2006). Aura MLS measurements include water vapor, ozone and carbon monoxide that are useful tracers of tropospheric and stratospheric air; these data have been used to document enhanced levels of carbon monoxide in the upper troposphere over the Asian monsoon (Li et al., 2005a; Filipiak et al., 2005) and also over the North American summer monsoon (Li et al., 2005b).

ACPD
14, 3169–3191, 2014

3 Results

The occurrence of the Tibetan anticyclone existed approximately for the seventh consecutive day from 6 to 22 August 2011 (Fig. 1). Temperatures within the anticyclone are lower due to adiabatic expansion of ascending air parcels. During summer, the elevated surface heat and the rising air over the plateau lead to anticyclonic circulation and divergence in the upper troposphere and the lower stratosphere, which occurs primarily due to adiabatic heating associated with deep convection over South Asia during summer (Yanai et al., 1992). It is likely that cold temperature anomalies within the anticyclone at 100 hPa are primarily a dynamical response to enhanced convection (Park et al., 2007).

Figure 2 show the vertical profiles of aerosol extinction coefficients measured at Naqu during 6–26 August 2011, along with the daily mean profiles of temperature. The measurements display relatively high aerosol extinction coefficients in the UTLS, which are 2 factors higher than those at altitudes below and close to (even higher than, such as on 6 and 12 August) molecular scattering coefficients at the same altitude. The highest aerosol extinction coefficients in the UTLS generally located at 18–19 km altitudes, which are 1–2 km higher than the tropopause. Tropopause temperatures ranged from −70 °C to −80 °C, and the height of the tropopause varied from 80 hPa to 100 hPa (from 17 km to 18 km), during the observational period. Moreover, such relatively high aerosol extinction coefficients could extend over broad layers, ranging approximately 3–4 km.

In these cases, there were interesting temporal change in maximum extinction coefficients of the aerosol layer and the tropopause temperatures, as shown in Fig. 3. The maximum extinction coefficients looks like anti-correlated with the tropopause temperatures. The increased aerosol extinction coefficients usually accompanied with the decreasing tropopause temperatures along the time series. The maximum extinction coefficient of these cases is 2.40 m^{-1} on 12 August, when the tropopause temperature is −76.0 °C, being the lowest compared with the other cases. The minimum extinc-

ACPD
14, 3169–3191, 2014

tion coefficient of these cases is 0.87 m^{-1} on 26 August, corresponding the highest tropopause temperature of −72.3 °C.

There are two possible ways for the decreasing tropopause temperatures to affect the enhancement of high aerosol extinction. One way is the low temperatures due to adiabatic cooling of ascending air parcels induced by deep convective activities, which result in the direct transportation of natural and/or anthropogenic emissions from atmospheric boundary layer over the Tibetan Plateau. The decreasing temperature at the tropopause is generally associated with the enhancement in deep convective activities over the Tibetan Plateau. The low OLR has been treated as an indicator of the organized deep convective activity in the troposphere (Fujiwara et al., 2009). Figure 4 compares nighttime mean maximum aerosol extinction coefficients in UTLS with the OLR convection proxy over the Tibetan Plateau in August 2011. The enhancement of aerosols near the tropopause appears to be well correlated with the changes in OLR (r^2 = 0.77) without evidence of substantial time lags. According to the period of occurrence of aerosol layers in UTLS, the continuous lidar observation can be split into two stages: 6 to 12 (S1) and 22 to 26 (S2) August 2011 for the continuous maintenance stages of aerosol layer. These two stages might be caused by the different deep convective systems due to an apparent time interval of about 10 days. Additionally, the existence of low clouds in those days might obstruct significantly adiabatic cooling of ascending air parcels and vertical transportation of aerosol in lower troposphere, resulting in different variation of aerosol layer with intensity of deep convective activity in the two continuous maintenance stages of aerosol layer. The relationships of aerosol extinction coefficients and OLR in two continuous stages are also shown in Fig. 4 with correlation coefficient of 0.78 and 0.86 for S1 and S2, respectively, suggesting the possibility that the tropopause aerosol enhancement associates with the upward transport of aerosols in deep convective systems over the Tibetan Plateau. The overshooting deep convection could directly influence the aerosol concentration at this level. Using daily NCEP data and monthly SAGE data, Cong et al. (2001) calculated the interannual change of the aerosol and ozone in 100 hPa, and they proposed that the atmospheric

ACPD
14, 3169–3191, 2014

masses passing over the tropopause over the Tibet Plateau and its neighboring areas might possibly carry the aerosol particles of middle or lower troposphere into the vicinity of the tropopause and result in an increase of the aerosol loading near the tropopause. Yin et al. (2012) used a cloud resolving model coupled with a spectral bin microphysical scheme to investigate the effects of deep convection on the concentration and size distribution of aerosol particles within the upper troposphere, and found that aerosols originating from the boundary layer can be more efficiently transported upward, as compared to those from the mid-troposphere, due to significantly increased vertical velocity through the reinforced homogeneous freezing of droplets.

Similarly, the temporal variation trend of aerosol layer in UTLS altitude during the nighttime period further indicated that the tropopause aerosol enhancement associates with the upward transport of aerosols in deep convective systems over the Tibetan Plateau. Figure 5 shows the nighttime cycle of maximum extinction coefficient (MEC), aerosol layer depth (ALD) and AOD of the aerosol layer from local time 20:00 to 06:00, hourly averaged for all cases. An obvious temporal variation of the three parameters can be seen from this figure. Both maximum extinction coefficient and aerosol layer depth increased drastically from 20:00 LT and reached maximum until 00:00 LT. AOD increased more drastically with peak at 23:00 LT. The three parameters decreased almost stably until the morning (06:00 LT) in spite of slightly oscillation at 02:00 LT and 04:00 LT. It should be noted that nighttime variations in aerosol layer in UTLS are first discussed in this paper have not been addressed in previous studies as far as we know. Unfortunately, the high resolution of temporal variation in tropopause temperatures cannot be measured in the absence of radiosondes. However, the nighttime variation trend of aerosol layer in UTLS altitude characterized by single peak at midnight can further support the conclusion that diurnal cycles of deep convective activity should be the major factor in the aerosol concentration above the tropopause, because deep convective systems generally start to develop in the early afternoon and continuously transport air with high aerosol concentrations vertically from the lower troposphere to the near tropopause until the night. As found by Nesbitt and Zipser (2003),

ACPD
14, 3169–3191, 2014

who analyzed a comprehensive 3 yr database of precipitation features, some large size Mesoscale Convective Systems (MCS) may keep developing through the night even until the early morning. Because of horizontal mixing and less vertical transport with less frequent deep convection in the morning, the concentrations of aerosol decrease and may reach their minima near morning. These convective systems may directly inject aerosol into the UTLS during afternoon until the mid night and lead to a higher concentration of aerosol around 00:00 LT over the Tibetan Plateau. The temporal variation of aerosols accumulated in UTLS induced by deep convective activities over the Tibetan Plateau can be verified by the similar observation of carbon monoxide (CO) near the tropical tropopause (Liu and Zipser, 2009) and the model investigation about the roles of deep convection in the Tropical Tropopause Layer (TTL) (Kubokawa et al., 2012).

The other way for the decreasing tropopause temperatures to affect the enhancement of high aerosol extinction is the enlargement of pre-existing and/or vertically-transported aqueous solution droplets induced by adiabatic cooling and hydration of the air associated with deep convection. It has been verified that deep convection over the Tibetan Plateau is likely to be a primary pathway for water vapor from the maritime boundary layer (e.g., Indian Ocean, South China Sea). Dessler and Sherwood (2004) have also suggested that convective transport plays a key role for the accumulation of water vapor near the tropopause, resulting in an increase of H_2O mixing ratio by more than 5 ppmv near the tropopause (Gettelman et al., 2004; Park et al., 2004; Fu et al., 2006). But Tobo et al. (2007) used a growth model to calculate the possible growth under given atmospheric conditions assuming the existence of liquid solutions at equilibrium with respect to H_2O, H_2SO_4 and HNO_3, and found that aerosol growth is sensitive to H_2O mixing ratios. In fact, the H_2O mixing ratios near the tropopause and aerosol layer from Vaisala RS92 radiosondes released in 6, 8 11 and 23 August 2011 are not more than 2 ppmv, obviously less than the previous observations, as shown in Fig. 6. In consequence, the effects of gas-to-particle conversion from liquid solutions

ACPD
14, 3169–3191, 2014

would likely be secondary to the enhancement of high tropopause aerosol extinction in these cases.

The continuous variation of water vapor distribution observed by satellite, despite lower vertical resolution, might also be used to investigate the contribution of liquid solutions conversion to the enhancement of high tropopause aerosol extinction. Figure 7 shows the time series of water vapor profile derived from MLS, tropopause level from sounder temperature profiles, and the altitude of daily mean maximum aerosol extinction coefficients in this region. It can be clearly seen that almost all the abundant water vapor transported by deep convective systems are concentrated below 120 hPa altitude (about 15 km). Meanwhile, the temporal correlation of extinction coefficients in aerosol layer with water vapor from day to day is weak with correlation coefficient of 0.36, suggesting that it is impossible that the enhanced tropopause aerosol is due to condensation of water vapor.

4 Conclusion

In this study, we observed significantly increased aerosol extinction coefficients in UTLS over the Tibetan Plateau by continuous measurements by MPL during summer 2011. The highest aerosol extinction coefficients in the UTLS generally located in 18–19 km m.s.l., 1–2 km higher than the tropopause, with broad layer depth ranging approximately 3–4 km. Interestingly, the maximum extinction coefficients are found to be increased with the decreasing tropopause temperatures. Nighttime mean maximum aerosol extinction coefficients in UTLS are also shown to be strongly coherent with the OLR convection proxy. Appearance of deep transport from the most intense convection is considered to be important factors to explain the enhancement of tropopause aerosols observed in summer over the Tibetan Plateau. Hour-to-hour variations in aerosol layer in UTLS over the Tibetan Plateau are investigated in this study for the first time, and results show a significant peak at midnight. This further verifies that deep convection plays an important role in the aerosol accumulation in UTLS over the

ACPD
14, 3169–3191, 2014

Tibetan Plateau. Deficiency in water vapor in UTLS indicates that the effects of gas-to-particle conversion from liquid solutions would likely be secondary to the enhancement of high tropopause aerosol extinction in these cases.

It is must be noted that our interpretations are based on a short time observation. It is difficult to conclude that either one of the two processes is dominant due to lack of observations for trace gases. If further observations with more frequent soundings of water vapor and trace gases can be performed to investigate a correlation of high aerosol extinction with ambient temperatures, water vapor, trace gases, liquid solutions and transport processes, the result will be helpful in validating origination and mechanism of the enhanced aerosol extinction in UTLS.

Acknowledgements. This study was supported by Special Funds for Meteorological Research in the Public Interest (Grant Numbers: GYHY201106023, GYHY201006047), the National Natural Science Foundation of China (NSFC, Grant Numbers: 40705013, 40975012 and 41175020), the Shanghai Science and Technology Committee Research Special Funds (Grant Number: 10JC1401600). We thank all TOAR team members and the staff from the Tibet Meteorological Service for assisting our experiment work. The authors gratefully acknowledge the NOAA/OAR/ESRL PSD, Boulder, Colorado, USA, for providing the interpolated OLR data on their web site http://www.cdc.noaa.gov/.

References

Borrmann, S., Solomon, S., Avallone, L., Toohey, D., and Baumgardner, D.: On the occurrence of ClO in cirrus clouds and volcanic aerosol in the tropopause region, Geophys. Res. Lett., 24, 2011–2014, 1997.

Campbell, J. R., Hlavka, D. L., Welton, E. J., Flynn, C. J., Turner, D. D., Spinhirne, J. D., Scott, V. S., and Hwange, I. H.: Full-time, eye-safe cloud and aerosol lidar observation at Atmospheric Radiation Measurement program sites: instruments and data processing, J. Atmos. Ocean. Tech., 19, 431–442, doi:10.1175/1520-0426(2002)019<0431:FTESCA>2.0.CO;2, 2002.

Chazette, P.: The monsoon aerosol extinction properties at Goa during INDOEX as measured with lidar, J. Geophys. Res., 108, 4187, doi:10.1029/2002JD002074, 2003.

ACPD
14, 3169–3191, 2014

Cong, C. H., Li, W. L., and Zhou, X. J.: Atmospheric mass exchange between the troposphere stratosphere over the Tibetan Plateau and its neighboring regions, Science Bulletin, 46, 1914–1918, 2001.
Dessler, A. E. and Sherwood, S. C.: Effect of convection on the summertime extratropical lower stratosphere, J. Geophys. Res., 109, D23301, doi:10.1029/2004JD005209, 2004.
Dethof, A., O'Neill, A., Slingo, J. M., and Smit, H. G. J.: A mechanism for moistening the lower stratosphere involving the Asian summer monsoon, Q. J. Roy. Meteor. Soc., 125, 1079–1106, 1999.
Fernald, F. G.: Analysis of atmospheric lidar observations: some comments, Appl. Optics, 23, 652–653, 1984.
Filipiak, M. J., Harwood, R. S., Jiang, J. H., Li, Q., Livesey, N. J., Manney, G. L., Read, W. G., Schwartz, M. J., Waters, J. W., and Wu, D. L.: Carbon monoxide measured by the EOS Microwave Limb Sounder on Aura: first results, Geophys. Res. Lett., 32, L14825, doi:10.1029/2005GL022765, 2005.
Fu, R., Hu, Y., Wright, J. S., Jiang, J. H., Dickinson, R. E., Chen, M., Filipiak, M., Read, W. G., Waters, J. W., and Wu, D.: Short circuit of water vapor and polluted air to the global stratosphere by convective transport over the Tibetan Plateau, P. Natl. Acad. Sci. USA, 103, 5664–5669, 2006.
Hanson, D. R., Ravishankara, A. R., and Solomon, S.: Heterogeneous react ions in sulfuric acid aerosols: a framework for model calculations, J. Geophys. Res., 99, 3615–3629, 1994.
Fujiwara, M., Iwasaki, S., Shimizu, A., Inai, Y., Shiotani, M., Hasebe, F., Matsui, I., Sugimoto, N., Okamoto, H., Nishi, N., Hamada, A., Sakazaki, T., and Yoneyama, K.: Cirrus observations in the tropical tropopause layer over the western Pacific, J. Geophys. Res., 114, D09304, doi:10.1029/2008JD011040, 2009.
Gettelman, A., Salby, M. L., and Sassi, F.: Distribution and influence of convection in the tropical tropopause region, J. Geophys. Res., 107, D104080, doi:10.1029/2001JD001048, 2002.
Highwood, E. J. and Hoskins, B. J.: The tropical tropopause, Q. J. Roy. Meteor. Soc., 124, 1579–1604, 1998.
Hoskins, B. J. and Rodwell, M. J.: A model of the Asian summer monsoon. Part I: The global scale, J. Atmos. Sci., 52, 1329–1340, 1995.
Jackson, D. R., Driscoll, S. J., Highwood, E. J., Harries, J. E., and Russell, J. M.: Troposphere to stratosphere transport at low latitudes as studied using HALOE observations of water vapour 1992–1997, Q. J. Roy. Meteor. Soc., 124, 169–192, 1998.

ACPD
14, 3169–3191, 2014

Keim, E. R., Fahey, D. W., Del Negro, L. A., Woodbridge, E. L., Gao, R. S., Wennberg, P. O., Cohen, R. C., Stimpfle, R. M., Kelly, K. K., Hintsa, E. J., Wilson, J. C., Jonsson, H. H., Dye, J. E., Baumgardner, D., Kaw, S. R., Salawitch, R. J., Proffitt, M. H., Loewenstein, M., Podolske, J. R., and Chan, K. R.: Observations of large reductions in the NO/NOy ratio near the mid-latitude tropopause and the role of heterogeneous chemistry, Geophys. Res. Lett., 23, 3223–3226, 1996.

Kim, Y. S., Shibata, T., Iwasaka, Y., Shj, G., Zhou, X., Tamuraa, K., and Ohashi, T.: Enhancement of aerosols near the cold tropopause in summer over Tibetan Plateau: lidar and balloon-borne measurements in 1999 at Lhasa, Tibet, China, in: Lidar Remote Sensing for Industry and Environment Monitoring III, edited by: Singh, U. N., Itabe, T., and Liu, Z., Proceedings of SPIE, Hangzhou, China, 4893, 496–503, 2003.

Kubokawa, H., Fujiwara, M., Nasuno, T., Miura, M., Yamamoto, M. K., and Satoh, M.: Analysis of the tropical tropopause layer using the Nonhydrostatic Icosahedral Atmospheric Model (NICAM): 2. An experiment under the atmospheric conditions of December 2006 to January 2007, J. Geophys. Res., 117, D17114, doi:10.1029/2012JD017737, 2012.

Li, Q., Jiang, J., Wu, D., Read, W., Livesey, N., Waters, J., Zhang, Y., Wang, B., Filipiak, M., Davis, C., Turquety, S., and Wu, S.: Convective outflow of South Asian pollution: a global CTM simulation compared with EOS MLS observations, Geophys. Res. Lett., 32, L14826, doi:10.1029/2005GL022762, 2005a.

Li, Q., Jacob, D., Park, R., Wang, Y., Heald, C., Hudman, R., Yantosca, R., Martin, R., and Evans, M.: North American pollution outflow and the trapping of convectively lifted pollution by upper-level anticyclone, J. Geophys. Res., 110, D10301 doi:10.1029/2004JD005039, 2005b.

Li, W. L. and Yu, S. M.: The characteristics of aerosol spatial and temporal distribution, radiation forcing and climate effect by numerical simulation over the Tibetan Plateau, Sci. China Ser. D, 31, 300–307, 2001.

Liebmann, B. and Smith, C. A.: Description of a complete (interpolated) outgoing longwave radiation dataset, B. Am. Meteorol. Soc., 77, 1275–1277, 1996.

Liu, C. and Zipser, E. J.: Implications of the day versus night differences of water vapor, carbon monoxide, and thin cloud observations near the tropical tropopause, J. Geophys. Res., 114, D09303, doi:10.1029/2008JD011524, 2009.

Miloshevich, L. M., Vömel, H., Whiteman, D. N., Lesht, B. M., Schmidlin, F. J., and Russo, F.: Absolute accuracy of water vapor measurements from six operational radiosonde types

ACPD
14, 3169–3191, 2014

launched during AWEX-G and implications for AIRS validation, J. Geophys. Res., 111, D09S10, doi:10.1029/2005JD006083, 2006.
NASA: US Standard Atmosphere Supplements, US Govt. Print. Off., Washington DC, 1976.
Nesbitt, S. W. and Zipser, E. J.: The diurnal cycle of rainfall and convective intensity according to three years of TRMM measurements, J. Climate, 16, 1456–1475, 2003.
Park, M., Randel, W. J., Kinnison, D. E., Garcia, R. R., and Choi, W.: Seasonal variation of methane, water vapor, and nitrogen oxides near the tropopause: satellite observations and model simulations, J. Geophys. Res., 109, D03302, doi:10.1029/2003JD003706, 2004.
Park, M., Randel, W. J., Gettelman, A., Massie, S. T., and Jiang, J. H.: Transport above the Asian summer monsoon anticyclone inferred from Aura Microwave Limb Sounder tracers, J. Geophys. Res., 112, D16309, doi:10.1029/2006JD008294, 2007.
Rosenlof, K. H., Tuck, A. F., Kelly, K. K., Russell III, J. M., and McCormick, M. P.: Hemispheric asymmetries in water vapor and inferences about transport in the lower stratosphere, J. Geophys. Res., 102, 13213–13234, 1997.
Solomon, S.: Stratospheric ozone depletion: a review of concept and history, Rev. Geophys., 37, 275–316, 1999.
Solomon, S., Borrmann, S., Garcia, R. R., Portmann, R., Thomason, L., Poole, L. R., Winker, D., and McCormick, M. P.: Heterogeneous chlorine chemistry in the tropopause region, J. Geophys. Res., 102, 21411–21429, 1997.
Tobo, Y., Zhang, D., Iwasaka, Y., and Shi, G.: On the mixture of aerosols and ice clouds over the Tibetan Plateau: results of a balloon flight in the summer of 1999, Geophys. Res. Lett., 34, L23801, doi:10.1029/2007GL031132, 2007.
Vömel, H. H., Selkirk, L., Miloshevich, J., Valverde-Canossa, J., Valdes, J., and Diaz, J.: Radiation dry bias of the Vaisala RS92 humidity sensor, J. Atmos. Ocean. Tech., 24, 953–963, 2007.
Währn, J., Oyj, V., Rekikoski, I., Jauhiainen, H., and Hirvensalo, J.: New Vaisala Radiosonde RS92: Testing and Results from the Field, Eighth Symposium on Integrated Observing and Assimilation Systems for Atmosphere, Oceans, and Land Surface, Seattle, USA, 13 January 2004, 2004.
Waters, J. W., Froidevaux, L., Harwood, R. S., Jarnot, R. F., Pickett, H. M., Read, W. G., Siegel, P. H., Cofield, R. E., Filipiak, M. J., Flower, D. A., Holden, J. R., Lau, G. K., Livesey, N. J., Manney, G. L., Pumphrey, H. C., Santee, M. L., Wu, D. L., Cuddy, D. T., Lay, R. R., Loo, M. S., Perun, V. S., Schwartz, M. J., Stek, P. C., Thurstans, R. P., Boyles, M. A., Chandra, K. M.,

ACPD
14, 3169–3191, 2014

Chavez, M. C., Chen, G. S., Chudasama, B. V., Dodge, R., Fuller, R. A., Girard, M. A., Jiang, J. H., Jiang, Y., Knosp, B. W., LaBelle, R. C., Lam, J. C., Lee, K. A., Miller, D., Oswald, J. E., Patel, N. C., Pukala, D. M., Quintero, O., Scaff, D. M., Van Snyder, W., Tope, M. C., Wagner, P. A., and Walch, M. J.: The Earth Observing System microwave limb sounder (EOS MLS) on the Aura satellite, IEEE T. Geosci. Remote, 44, 1075–1092, 2006.

Welton, E. J., Voss, K. J., Gordon, H. R., Maring, H., Smirnov, A., Holben, B. N., Schmid, B., Livingston, J. M., Russell, P. B., Durkee, P. A., Formenti, P., and Andreae, M. O.: Ground-based lidar measurements of aerosols during ACE-2: lidar description, results, and comparisons with other ground-based and airborne measurements, Tellus B, 52, 636–651, 2000.

Wu, L.: Short circuit of water vapor and polluted air to the global stratosphere by convective transport over the Tibetan Plateau, P. Natl. Acad. Sci. USA, 103, 5664–5669, 2006.

Yanai, M., Li, C., and Song, Z.: Seasonal heating of the Tibetan Plateau and its effects on the evolution of the Asian summer monsoon, J. Meteorol. Sci. Jpn., 70, 319–351, 1992.

Yin, Y., Chen, Q., Jin, L., Chen, B., Zhu, S., and Zhang, X.: The effects of deep convection on the concentration and size distribution of aerosol particles within the upper troposphere: a case study, J. Geophys. Res., 117, D22202, doi:10.1029/2012JD017827, 2012.

ACPD
14, 3169–3191, 2014

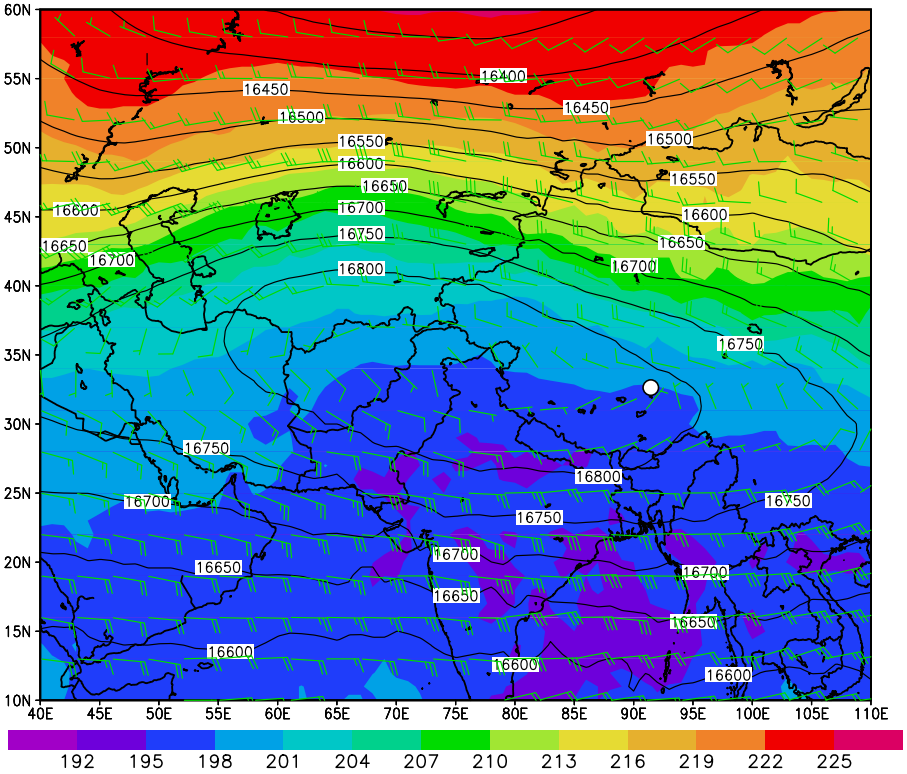

Fig. 1. NCEP analyzed wind field, geopotential height and temperature at 100 hPa altitude on 22 August 2011. The circle is lidar site on Naqu, Tibet.

ACPD
14, 3169–3191, 2014

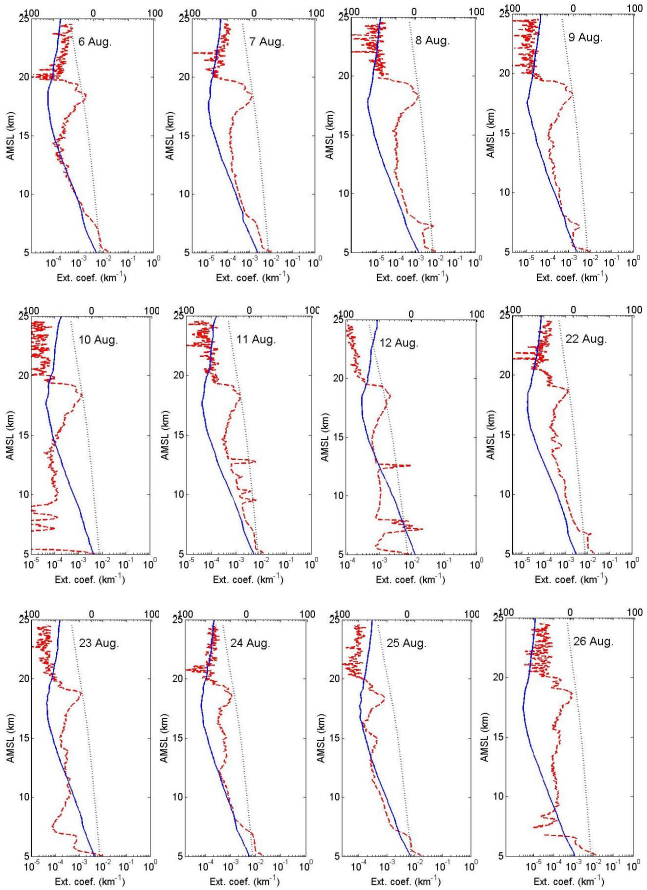

Fig. 2. The nighttime mean aerosol extinction coefficient profiles (dashed line) from MPL and Rayleigh scattering coefficient profiles (dotted line) of single days over the Tibetan Plateau in August 2011. The daily mean profiles of temperature (solid line) from the two radiosondes each day are overlaid to indicate the altitude of the tropopause (~ 18 km m.s.l.).

ACPD
14, 3169–3191, 2014

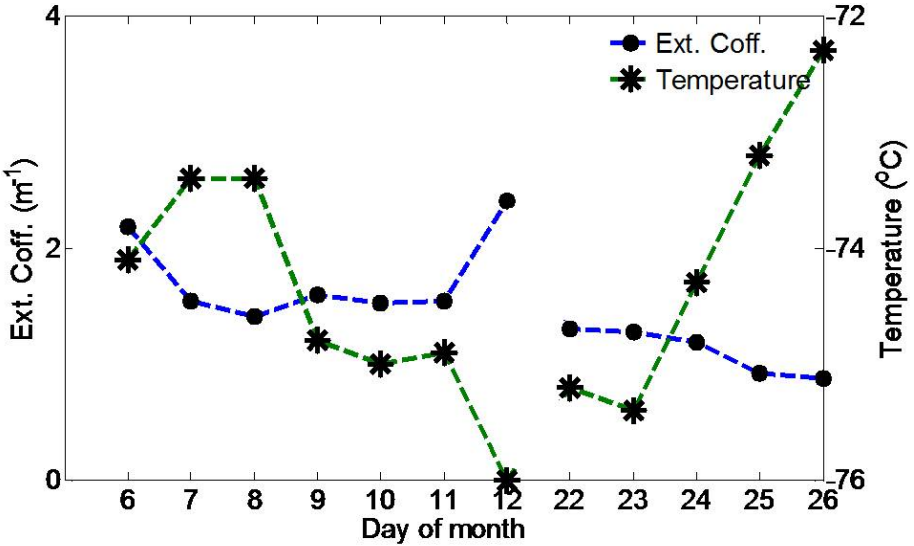

Fig. 3. The time series of maximum extinction coefficient in the aerosol layers and temperature at the tropopause over the Tibetan Plateau day-on-day in August 2011.

ACPD
14, 3169–3191, 2014

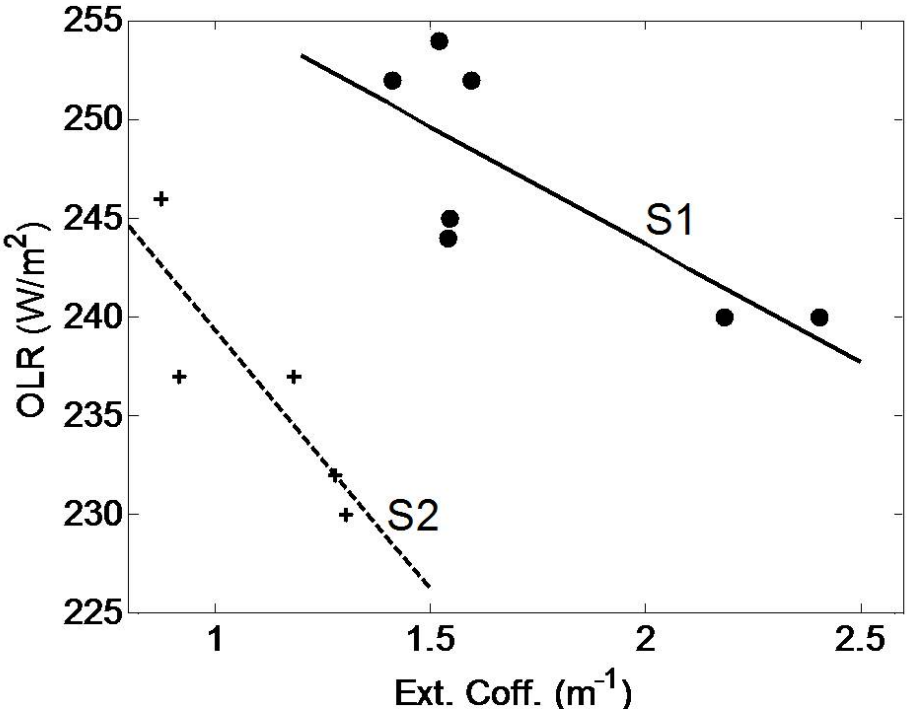

Fig. 4. Nighttime mean maximum extinction coefficient in the aerosol layer vs. OLR. The dots represent the data for 6–12 August (S1) and the pluses for 22–26 August 2011 (S2).

ACPD
14, 3169–3191, 2014

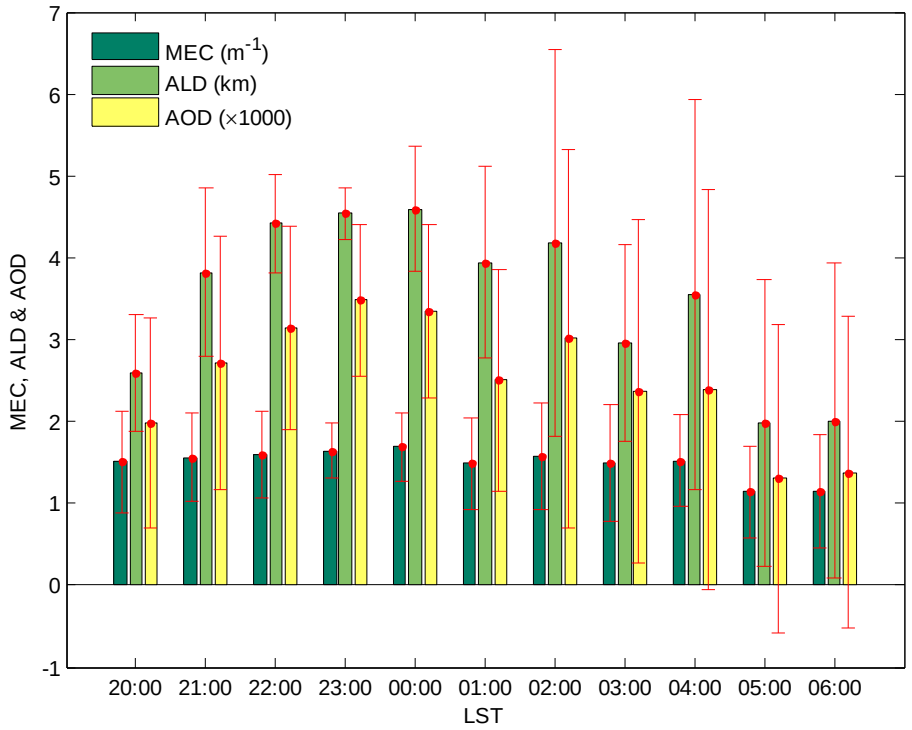

Fig. 5. The temporal variation of maximum extinction coefficient (MEC), aerosol layer depth (ALD) and aerosol optical depth (AOD) of the aerosol layer from 20:00 to 06:00 local standard time (LST). The error bars correspond to the standard deviations.

ACPD
14, 3169–3191, 2014

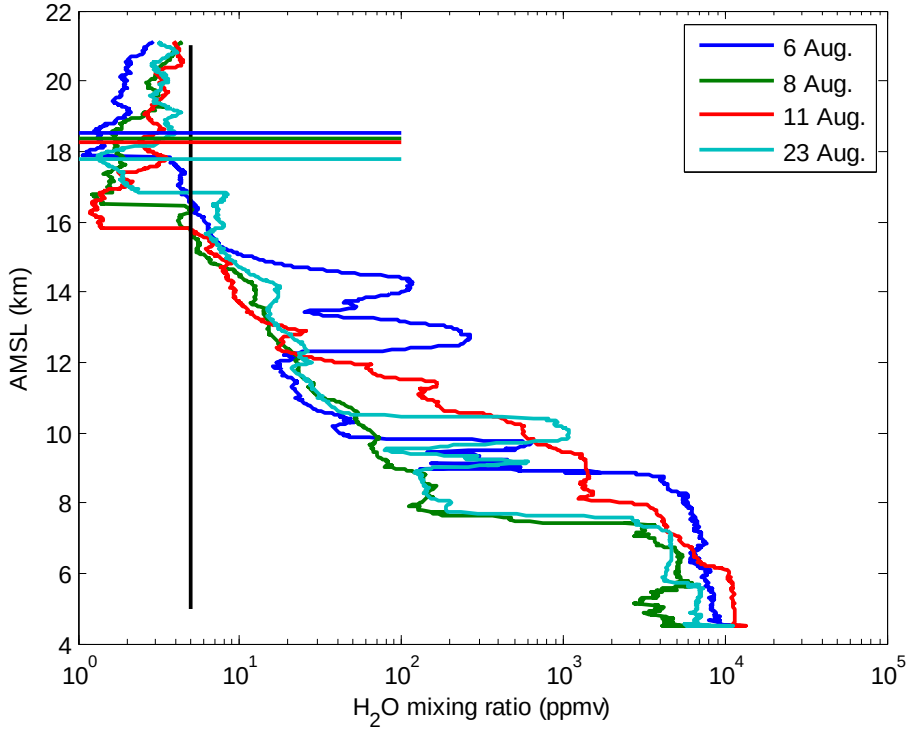

Fig. 6. Vertical profiles of water vapor from Vaisala RS92 radiosondes released in 6, 8, 11 and 23 August 2011, respectively. The black line along *y* axis represents the 5 ppmv of water vapor mixing ratio. The color lines along *x* axis are the altitudes with the maximum extinction coefficient of aerosol layers for each day.

ACPD
14, 3169–3191, 2014

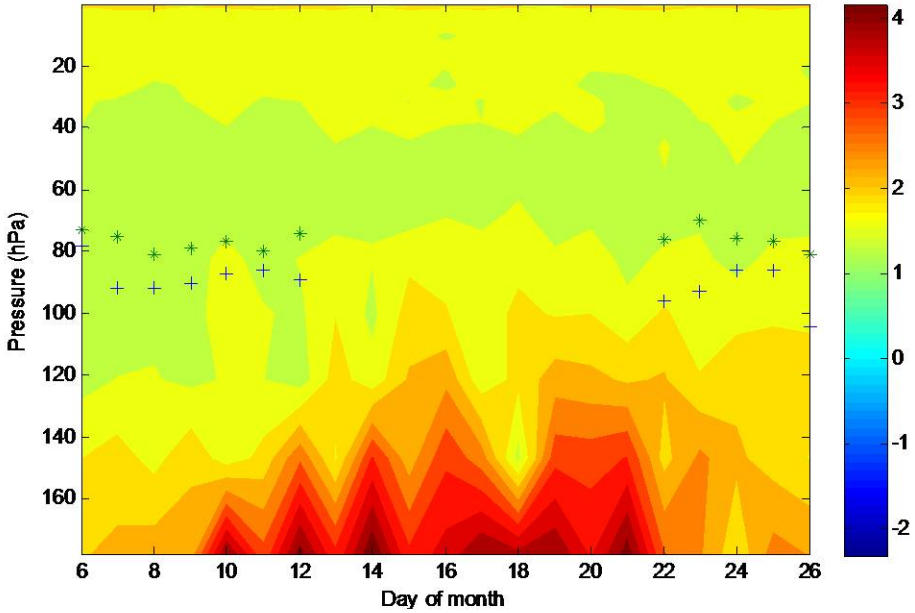

Fig. 7. Altitude-time distributions of MLS water vapor (ppmv, color bar in natural logarithm) from 6 to 26 August 2011. Stars indicate the layer with nighttime mean maximum extinction coefficient and pluses stand for the tropopause level of each day, respectively.

ACPD
14, 3169–3191, 2014